CHEMICAL ENGINEERING TRANSACTIONS
VOL. 120, 2025
A publication of AIDIC
The Italian Association of Chemical Engineering
Online at www.cetjournal.it
Guest Editors: Bing Shen How, Viknesh Andiappan, Denny K.S. Ng, Hon Loong Lam, Petar S. Varbanov

ISBN 979-12-81206-21-2; **ISSN** 2283-9216
DOI: 10.3303/CET25120036

Assessment of the Thermocline Thermal Energy Storage Tank Thermal Expansion

Karem Elsayed Elfeky[a,*], Abubakar Gambo Mohammed[b], Qiuwang Wang[c], Kun Ge[a]

[a]College of Power and Energy Engineering, Harbin Engineering University, Harbin 150001, China
[b]Institute of Sustainable Energy, Universiti Tenaga Nasional, Putrajaya Campus, 43000 Kajang, Selangor, Malaysia
[c]Key Laboratory of Thermo-Fluid Science and Engineering, Ministry of Education, School of Energy and Power Engineering, Xi'an Jiaotong University, Xi'an, Shaanxi 710049, P.R. China
elfeky_karem@hrbeu.edu.cn

A packed-bed thermocline tank offers a cost-effective solution for thermal energy storage in concentrating solar power (CSP) plants. However, structural issues caused by thermal expansion have limited its deployment. This study develops a comprehensive model of a multilayer thermocline tank incorporating a composite steel shell with dual-layer insulation and encapsulated phase change materials (PCMs) suspended in molten salt. The model independently accounts for the varying thermal properties of molten salt and PCMs to evaluate the thermo-mechanical performance of the tank. Results show that the section of the tank wall exposed to high temperature expands by 30.5 % as charging time increases from 50 to 300 min. Additionally, the equivalent stress distribution exhibits multiple peaks due to thermocline movement, reaching 184.7 MPa at 208 min. The study demonstrates the importance of thermal expansion analysis for improving structural integrity and optimizing tank design in high-temperature CSP systems.

1. Introduction

One of the most important sources of renewable energy is solar energy because it is free and, with time, it is inexhaustible and has been widely used through photovoltaic or concentrating solar power (CSP) plants (Khan et al., 2025). Thermal energy storage (TES) has attracted considerable attention from researchers worldwide because of its effectiveness in terms of efficiency and cost for all solar energy applications at low, medium, and high temperatures (Elfeky et al., 2024). Thermochemical, sensible, and latent heat storage can be used in three different ways to store thermal energy. At present, thermochemical storage of heat is still undergoing laboratory investigations in labs, while sensible heat storage has been widely spread in industrial applications (Shankaranarayanan et al., 2025). Latent heat storage as TES technology is better than sensible heat storage because it has a high storage density and can store/recover energy at a very low difference in temperature between the molten salt and the phase change materials (PCMs) particles (Elfeky et al., 2022).
To further improve performance, some studies attempted to design a cascaded tank. For example, Elfeky et al. (2020) optimised the volume fraction of PCM of a cascaded layer tank, finding that the optimal performance of a higher volume fraction in the bottom layer results in optimal performance. Gao et al. (2023) optimised a cascaded tank, finding that the ideal charging time can increase by 7 % compared with a single tank. Zhao et al. (2018) found that an increase in the threshold temperature during charging and a decrease during discharging can enhance the capacity factor of the tank. Guo et al. (2023) optimised the volume ratio of the three PCM layer heights to 3:6:1, resulting in a 6.96 % enhancement of the cyclic heat transfer rate compared with a single tank. For the one-tank packed-bed TES system filled with sensible thermal storage materials (i.e., quartzite, rock, silica, and sand), Flueckiger et al. (2012) numerically analysed the hoop stress of the steel wall enveloped by firebrick and ceramic when the wall temperature properties were numerically obtained. Meanwhile, Iverson et al. (2017) experimentally revealed the thermal ratcheting property of the packed bed tank

Paper Received: 06 May 2025; Revised: 4 September 2025; Accepted: 11 September 2025
Please cite this article as: Elfeky K.E., Mohammed A.G., Wang Q., Ge K., 2025, Assessment of the Thermocline Thermal Energy Storage Tank Thermal Expansion, Chemical Engineering Transactions, 120, 211-216 DOI:10.3303/CET25120036

when quartzite and silica were adopted as the filler materials, and the parameter effects on stress performance were measured.
From the literature review, it can be concluded that great efforts have been focused on mechanical investigation to improve the safety of the single-layer thermocline tank. However, for the multilayer thermocline tank in elevated temperature service, few papers focus on mechanical investigation studies, which would obviously affect the service life of the TES system. Meanwhile, it is known that when the evaluation of mechanical damage is analysed, the key parameters, such as equivalent stress and equivalent strain, are influenced significantly by the thermal performance of the thermocline tank. This paper aims to estimate the mechanical damage of a multilayer thermocline TES tank. This work can provide insights into the optimization design of the multilayer TES configurations to improve the safety performance in service life.

2. Numerical formulation

The schematic diagram of the thermocline TES tank system, which uses three layers of PCMs with different thermo-physical properties, is shown in Figure 1(a). The TES thermocline tank system contains a cylindrical reservoir installed vertically with two outlets, the first at the top and the second at the bottom, which are used for the passing of the molten salt for the charging and discharging cycles, respectively. The thermocline tank is filled with three different layers of PCM particles with an equal radius and at different melting points. The molten salt passes through the spaces that exist between the capsules. At both the inlet and outlet, there is a distributor, and its function is to make the airflow uniformly through the packing region.

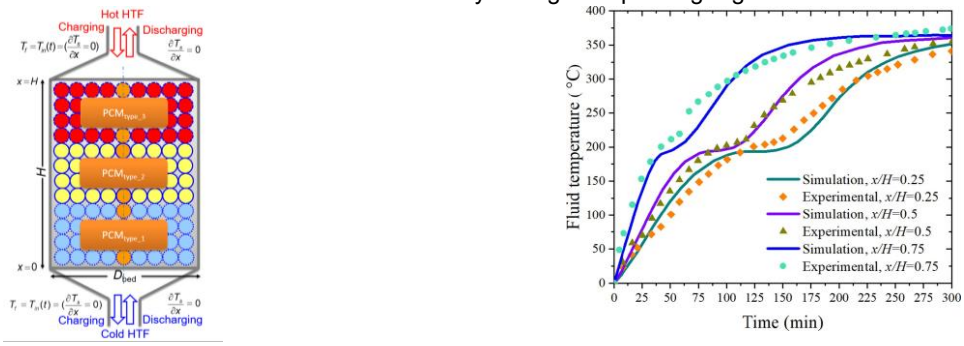

(a) (b)

Figure 1: (a) Schematic diagram of the packed-bed thermal-energy-storage system; (b) comparison between the present model's predicted heat-transfer-fluid (HTF) axial-temperature profile and the experimental data of Wang et al. (2022).

Three-stage packed bed PCMs, where the bed is divided equally into three axial sections, each PCM occupies 1/3 of the bed, and each section is filled with different PCM material, PCM type-1, PCM type-2, and PCM type-3 in sequence. The arrangements are considered in this case based on the PCM melting temperature, from high to low (PCM type-3, PCM type-2, PCM type-1). The spherical PCM capsules that are the subject of this study are encapsulated in an alumina shell. Table 1 summarises the PCMs properties of the packed bed thermal storage system.

Model description

In the present study, the dispersion-concentric (D-C) numerical model is used to study the dynamic behaviour of the TES tank and explain how the molten salt travels through the packing region. The thermocline TES tank in this model is considered a porous material consisting of separate capsules of the PCMs (Elfeky et al., 2018). The assumptions below are as follows: The inner and outer surfaces of the tank are completely insulated. The molten salt flows from the top inlet port into the bottom outlet port during charging and vice versa during discharging. The current numerical model considers all PCM capsules identical and divides them into equal spaces. It does not consider the distributors. The energy lost from the two ends of the thermocline tank is ignored due to its very small value (Elfeky et al., 2018). The thermophysical characteristics of the molten salt are determined by the inlet and exit temperature, $T_{ave} = (T_{in}+T_{ex})/2$ (.Operating between 288 and 565 °C, the heat transfer fluid utilized in the study is a blend of 60 % sodium nitrate ($NaNO_3$) and 40 % potassium nitrate (KNO_3) Elfeky et al., 2018).
The radiation heat transfer and heat generated within the thermocline TES tank have been neglected. The mathematical equations of the current numerical model that describe the heat transfer process between both

the molten salt and PCMs capsules are resolved based on the assumptions mentioned above: For the molten salt:

$$\varepsilon\rho_f c_{p,f}\frac{\partial T_f}{\partial t}+\varepsilon u_f\rho_f c_{p,f}\frac{\partial T_f}{\partial x}=\varepsilon\lambda_f\frac{\partial^2 T_f}{\partial x^2}+h_f\left(T_s-T_f\right)+h_w\left(T_w-T_f\right) \quad (1)$$

where T_f, T_s, and T_{inf} indicate the temperatures of heat fluid, solid PCM, and ambient temperature, which is assumed to be 23 °C, respectively, t is the time, ε is the packed-bed region's porosity, h_f is the interstitial heat transfer coefficient, U_W is the overall heat transfer coefficient, λ_f is the thermal conductivity of the fluid, u_f is the fluid inlet velocity, $c_{p,f}$ and ρ_f are the specific heat and density of fluid.
For the PCMs capsules:

$$(1-\varepsilon)\rho_s c_{p,s}\frac{\partial T_s}{\partial t}=(1-\varepsilon)\lambda_s\frac{\partial^2 T_s}{\partial x^2}+h_f\left(T_f-T_s\right) \quad (2)$$

The distribution of the temperature on the PCM capsule surface can be determined as follows:

$$\rho_s c_{p,s}\frac{\partial T_p}{\partial t}=\frac{1}{r^2}\frac{\partial}{\partial r}\left(\lambda_s r^2\frac{\partial T_p}{\partial r}\right) \quad (3)$$

where ρ_s, $c_{p,s}$, and λ_s are the density, the specific heat, and the thermal conductivity of the PCM material, respectively.

Table 1: PCMs properties (Elfeky et al., 2018).

Arrangement	PCMtype_1	PCMtype_2	PCMtype_3
Melting temperature, T_m (°C)	382.1	439.8	550
Solidification temperature, T_s (°C)	390.9	429.8	540.5
Latent heat of fusion, h_f (kJ/kg)	197.6	214.9	283
Latent heat of solidification, h_s (kJ/kg)	183.7	162.9	283
Solid density, ρ_s (kg/m³)	2,118	2,109	2,380
Liquid density, ρ_l (kg/m³)	1,607	1,604	2,380
Solid thermal conductivity, λ_s (W/m-K)	1.0	1.0	1.83
Liquid thermal conductivity, λ_l (W/m-K)	1.0	1.0	1.83
Solid specific heat capacity, $c_{p,s}$ (J/kg-K)	928	1,005	928
Liquid specific heat capacity, $c_{p,l}$ (J/kg-K)	1,035	1,096	928

To better describe the effects of structural form, mechanical load, and temperature distribution on the stress performance of the packed-bed tank, a transient three-dimensional mechanical model is further developed. The calculation region of the stress analysis model is conducted. In charging and discharging, due to the tank wallboard is always subjected to hydrostatic pressure and thermal stress. Thus, the stress, strain, and displacement expressions can be calculated based on the thermo-elastic theory. The governing equations of the stress analysis model are given as follows (Wu et al., 2017).
Constitutive equation:

$$\varepsilon_{x_i}=\frac{1}{E}(\sigma_{x_i}-\nu.\Theta)+\alpha\Delta T \quad (4)$$

where E stands for Young's modulus or modulus of elasticity, α for coefficient of thermal expansion, ΔT for temperature change from a reference temperature, v for Poisson's ratio, θ for sum of normal stresses in other directions, and ε_x for total strain in the x-direction and σ_x for normal stress in the x-direction.
Displacement equation:

$$(\lambda+G)\frac{\partial\theta}{\partial x_i}+G.\nabla^2 u_i-\frac{\alpha E}{1-2\nu}\frac{\partial(\Delta T)}{\partial x_i}=0 \quad (5)$$

Geometric equation:

$$\varepsilon_{x_i}=\frac{\partial u_i}{\partial x_i} \quad (6)$$

Strain coordination equation:

$$\nabla^2\sigma_{x_i}+\frac{1}{1+\nu}\frac{\partial^2\Theta}{\partial x_i^2}=-\alpha E\left[\frac{1}{1-\nu}\nabla^2(\Delta T)+\frac{1}{1+\nu}\frac{\partial^2(\Delta T)}{\partial x_i^2}\right] \quad (7)$$

where the shear elastic modulus and Ramet constant are denoted by G and λ, respectively. G = 0.5E/(1 + v) and λ = Ev/[(1 + v)(1-v)] and Pa is the volumetric strain.

Numerical approach

The packing region of the thermocline tank is sectioned into an equal number of control volumes. Moreover, the axial and the radial direction have been divided respectively into an equal number of sections (Nx) and (Rx), for all the current studied cases, as demonstrated in Figure 1(a). The progress of the heat exchange between the PCMs capsules and the molten salt is a function of the difference in temperature between them. By directly approximating the finite difference method within the fully implicit scheme, the (D-C) model equations that characterise the rate of heat transfer between the PCMs capsules and the HTF are solved using MATLAB. The First-order upwind method is used to solve both the advective and temporal terms in the mathematical equation (Eq(2)); simultaneously, the second-order central difference approach is used to solve the diffusion term. After the 3-D mechanical model is established by ICEM CFD, the cyclic temperature fields of the tank wall are rotated and mapped to the mechanical model based on the platform in ANSYS Workbench 19.0.

3. Results and discussion

In the present work, the thermal-mechanical behaviour of the TES thermocline tank is one of the important parameters for determining the power generation and the CSP efficiency. The thermocline TES tank, which included PCM capsules with a diameter of 0.0265 m and a porosity of 0.22, was designed to be 7.376 m high and 10.593 m in diameter. Each capsule had a 0.00045 m thick shell and a 13.94 w/(m·°C) thermal conductivity, with a 0.0508 m-thick tank wall. The heat transfer fluid, which circulated at a mass flow rate of 84.517 kg/s, was a molten salt mixture that contained 60 % $NaNO_3$ and 40 % KNO_3. With charging and discharging cut-off temperatures set at 398 °C and 495 °C, respectively, the system functioned between 288 °C and 565 °C.

3.1 Verification of the model

The accuracy of the current inquiry is evaluated by validating the results of the current study against the experimental works of Wang et al. (2022). The current study's geometry and that of the references under consideration are nearly identical. As in the references listed, the same operational parameters are applicable. Figure 1(b) demonstrates that there is adequate agreement between these two studies and the present study, demonstrating the accuracy of the numerical simulation.

3.2 Temperature profiles in a packed bed

Figure 2 displays the tank wall temperature profile along the bed for charging and discharging processes, respectively. To describe the mechanical damage time of the tank wall during charging and discharging cycles, the wall temperature variations along the height direction at different times in the cycle are displayed, as shown in Figure 2. It is found that the wall temperature varies with increasing charging time.

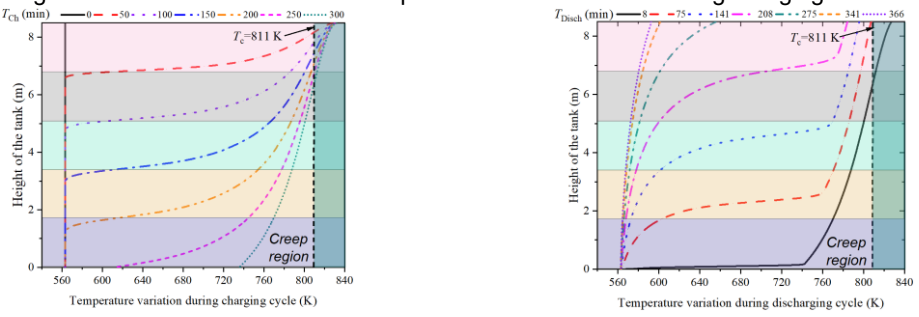

(a) (b)

Figure 2: The wall temperature profile along the bed during a) charging and (b) discharging processes.

3.3 Mechanical analysis

Figure 3 shows the tank wall deformation along the bed for the charging and discharging processes, respectively. The deformation of the tank wall progressively increases with extended charging time, reaching a

maximum displacement of 100 mm at the top section when the charging time tch reaches 300. In contrast, under the same conditions, the lower part of the tank wall exhibits significantly less deformation, with a measured displacement of 50 mm. This disparity highlights the non-uniform stress distribution across the tank structure during prolonged charging cycles. The upper section experiences a maximum contraction of 70 mm when the discharging time (tch) reaches 300. At the same time, the lower section demonstrates markedly less deformation under identical conditions, with a contraction measurement of 38.5 mm. This stark contrast in contraction magnitudes between the upper and lower regions underscores the non-uniform structural behavior of the tank wall during extended discharging cycles, likely influenced by localised thermal or mechanical stresses.

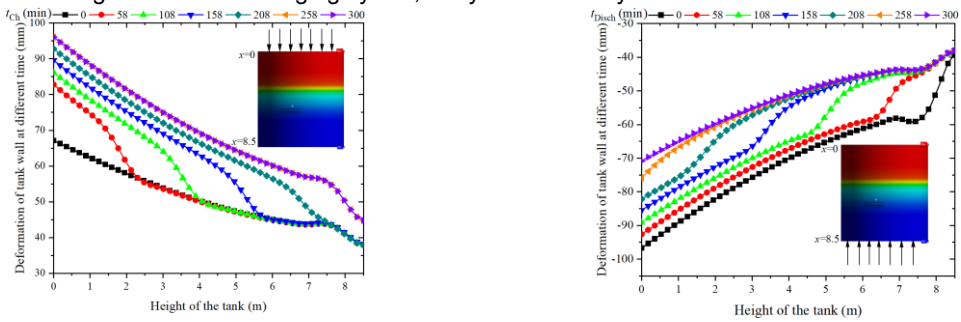

(a) *(b)*

Figure 3: Tank wall deformation along the bed for (a) charging processes and (b) discharging cycles.

Figure 4 shows the equivalent stress of the tank wall along the bed for the charging and discharging processes, respectively. The equivalent stress of the tank has several peaks during the charging process due to the thermocline zone movement, whereas the equivalent stress of the tank equals 166.6 MPa at t = 58 min, while the equivalent stress of the tank equals 184.7 MPa at t = 208 min. The equivalent stress in the wall of a tank is often higher at the lower part compared to the upper part due to the influence of hydrostatic pressure and thermocline zone movement. According to Figure 4, it is known that equivalent elastic stress has a significant influence on tank creep damage.

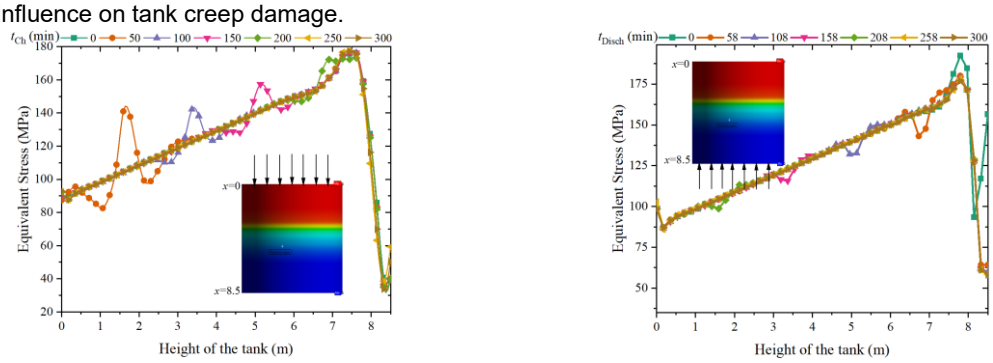

(a) *(b)*

Figure 4: Equivalent stress of the tank wall through (a) charging and (b) discharging processes.

Thus, the equivalent elastic stress variation of the tank wall during the charging and discharging operation is further discussed, as shown in Figures 4(a) and (b). The results show that the plastic yield could be induced because the peak stress is larger than the yield strength of 146 MPa of 321H stainless steel, and the yield phenomenon induced by stress concentration always occurs at the location connecting the bottom tank wall and tank base, and at the thermocline zone. The variation of charging time, even slightly, affects the location where peak stress happens.

4. Conclusions

This study presents a detailed numerical and mechanical model of a multilayer thermocline thermal energy storage tank using encapsulated PCMs and molten salt. The simulation results reveal that thermal expansion significantly affects the upper section of the tank wall, with temperature-dependent stress concentration increasing during extended charging and discharging cycles. The findings show that the tank wall experiences notable mechanical and thermal reactions throughout cycles of charging and draining. Temperature profiles

show that during extended charging, the upper tank wall above the creep barrier (811 K), with high-temperature exposure rising by 30.5 % between 50 and 300 min. In contrast, during discharging, this area of high temperature gradually disappears. The equivalent stress profiles exhibit several peaks as a result of thermocline movement, with stress values above the material's yield strength (146 MPa), especially in the thermocline zone and lower tank wall, signaling the possibility of creep damage and plastic deformation. These findings underscore the importance of incorporating thermo-mechanical analysis in TES tank design to prevent structural damage and enhance the operational reliability of CSP systems.

Acknowledgments

This work is financially supported by the Fundamental Research funds for the Central Universities of Harbin Engineering University (Grant No. 3072025CFJ0301) and the National Natural Science Foundation of China (No. 52306192).

References

Ahmed N., Elfeky, K.E., Qaisrani M.A., Wang, Q.W., 2019, Numerical characterization of thermocline behaviour of combined sensible-latent heat storage tank using brick manganese rod structure impregnated with PCM capsules. Solar Energy, 180, 243-256.

Elfeky K.E., Mohamed H., Mohammed A.G., Wenxiao C., Shaaban A., Qiuwang W., 2024, Performance optimization of the parabolic trough power plant using a dual-stage ensemble algorithm. Applied Thermal Engineering, 249, 123419.

Elfeky K.E., Mohammed A.G., Wang Q., 2022, Thermal performance evaluation of combined sensible-latent heat storage tank with a different storage medium. Chemical Engineering Transactions, 94, 1267–1272.

Elfeky K., Mohammed A.G., Ahmed N., Lu L., Wang Q., 2020, Thermal and economic evaluation of phase change material volume fraction for thermocline tank used in concentrating solar power plants. Applied Energy, 267, 115054.

Elfeky K.E., Ahmed N., Wang, Q., 2018, Numerical comparison between single PCM and multi-stage PCM based high temperature thermal energy storage for CSP tower plants. Applied Thermal Engineering, 139, 609-622.

Flueckiger S.M., Yang Z., Garimella S.V., 2012, Thermomechanical simulation of the Solar One thermocline storage tank. Journal of Solar Energy Engineering, 134(4), 041014.

Gao L., Dong L., Liu Z., Che D., Sun B., 2023, Thermal performance analysis and multi-objective optimization of thermal energy storage unit with cascaded packed bed in a solar heating system. Applied Thermal Engineering, 219, 119416.

Guo W., He Z., Mawire A., Zhang P., 2023, Parametric investigation of charging and discharging performances of a cascaded packed bed thermal energy storage system. Journal of Energy Storage, 57, 106229.

IIverson B.D., Bauer S.J., Flueckiger S.M., 2014, Thermocline bed properties for deformation analysis. Journal of Solar Energy Engineering, 136(4), 041002.

Khan M.I., Asfand F., Al-Ghamdi S.G., Bicer Y., Khan M., Faqooq M., Pesyridis A., 2025, Realizing the promise of concentrating solar power for thermal desalination: A review of technology configurations and optimizations. Renewable and Sustainable Energy Reviews, 208, 115022.

Shankaranarayanan S., Murugan D.K., 2025, Recent trends in thermal energy storage for enhanced solar still performance. Renewable and Sustainable Energy Reviews, 212, 115373.

Wu Z., Wu H.J., Han F., 2017, Elasticity, 2nd ed., Beijing Institute of Technology, Beijing.

Zhao B.C., Cheng M.S., Liu C., Dai Z.M., 2018, System-level performance optimization of molten-salt packed-bed thermal energy storage for concentrating solar power. Applied Energy, 226, 225–239.

Wang W., He X., Shuai Y., Qiu J., Hou Y., Pan Q., 2022, Experimental study on thermal performance of a novel medium-high temperature packed-bed latent heat storage system containing binary nitrate. Applied Energy, 309, 118433.